An Implementation of a Direction-Finding Antenna for Mobile Communications Using a Neural Network

Éric Charpentier, *Member, IEEE,* and Jean-Jacques Laurin, *Senior Member, IEEE*

***Abstract*—Direction-finding systems for radio signals are mostly used in mobile communications and avionics applications for antenna tracking or navigation purposes. In general, such systems require accurate calibration and may be sensitive to noise and external interference. In this paper, we will investigate the performance of a neural network-based direction-finding system under such conditions. The proposed topology is a hybrid one, combining a simple RF signal beamformer with a neural network. The training of the neural network is accomplished experimentally with a three-element antenna array by varying the beam's direction and the carrier frequency. The error on the estimated direction of arrival caused by the environment and training limitations are investigated.**

***Index Terms*—Mobile communication, navigation, neural network applications.**

I. Introduction

A standard technique used to accomplish beam tracking in mobile satellite communications is the monopulse system that uses a combining circuit to generate sum and difference outputs [1] that are processed to obtain the direction of arrival (DOA) of an incident beam. Typical implementations use two or four antenna elements [2]. Although such systems have a good performance over broad azimuth search sectors, they can give false results caused by resolution ambiguity when used in a full 360° azimuth sector. They also need calibration and careful antenna design.

In applications such as vehicular terminals used for satellite communications (e.g., MSAT, INMARSAT), the electrical dimensions of the antenna are of the order of one to two wavelengths, which leads to broad antenna beams. Therefore, there is no need for a high angular resolution tracking capability. Furthermore, the primary requirement is on the azimuth tracking since the vehicle constantly varies its orientation. In fact, the elevation variations are much less severe and a number of mechanically steered mobile terminals antennas described in the literature or commercially available [3], [4] do not implement elevation tracking.

The objective of this paper is to propose and validate experimentally the implementation of a simple direction finding (DF) system that can identify the azimuth direction of an incoming signal [5], therefore being suitable for mobile satellite communications. The system, including the antenna and a processing unit, must be easy to calibrate in order to adapt to varying environmental conditions and configurations. The proposed system implements an artificial neural network (NN) at the output of an antenna array's combining circuit. Such a system was recently described in [6] where it is shown that the hardware calibration used in a monopulse-based DF system can be avoided by implementing an NN-based DF processor. In this case, the effects of parasitic scattering and hardware imperfections are efficiently taken into account by training the system with a set of known DOA's. In [6], an eight-element linear array was used for DOA estimation in a 120° sector and a phase/amplitude receiver was measuring the RF signal at each antenna output. An accuracy of about 1°–2° was achieved. In certain applications where such an accuracy is not required, the number of elements can be smaller. One of our objectives in this work is to reduce complexity and, therefore, use an array of only three elements (which is the minimum possible number to avoid sign ambiguity) to achieve DOA prediction in a full 360° sector. Another objective being low cost, our system is not using a phase/amplitude receiver. Instead, a simple RF circuit (beamforming) combines the received signals and generates analog output power levels to be processed by an NN section performing DOA estimation. The task to accomplish during training of that network is not only to compensate for the imperfections of the antenna elements, but also for the nonideal behavior of the RF combining circuit, including the nonlinear response of the power detectors (diodes) and fluctuations of the incident wave's power level.

Other recent work featuring NN processing in DF applications can be found in the literature [7]–[9]. In these papers, NN's are used to accelerate the processing and reduce the computational complexity of the MUSIC superresolution algorithm. Also, ideal antennas and in-phase/quadrature receivers are assumed. Since our RF combining circuit gives power level of combined antenna signals instead of in-phase and quadrature levels, the MUSIC algorithm was not implemented in our system. Also, this paper will focus primarily on the case where only one wave is incident on the antenna array.

In [6]–[8], radial basis function (RBF) NN's are used whereas multilayer perceptrons (MLP) are used in [9]. In this work, the proposed NN is using a combination of adalines and MLP neurons. The reason for choosing MLP's instead of RBF's will be given in Section III.

In the foregoing sections, we will give the principles of the proposed antenna and neural networks and describe the training procedure. The performance of the proposed system as

Manuscript received July 27, 1998; revised March 10, 1999. This work was supported by NSERC and FCAR.

The authors are with Poly-Grames Research Center, Department of Electrical and Computer Engineering, Ecole Polytechnique de Montréal, Montreal, Quebec, Canada H3C 3A7.

Publisher Item Identifier S 0018-926X(99)07071-4.

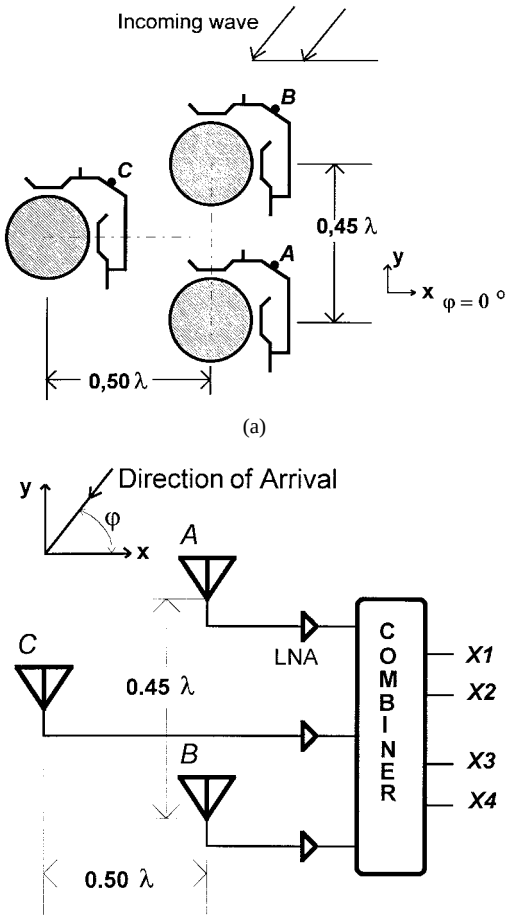

Fig. 1. (a) Physical layout of the DF antenna with three CP elements. (b) Array antennas followed by LNA (distances are given for a frequency of 1.55 GHz).

well as its sensitivity to frequency drift, noise, and interference caused by a second incoming wave will be investigated.

II. Antenna Array and RF Combining Network

The antenna used consists of an array of three horizontal printed circular patches as shown in Fig. 1. Each patch has a dual, in-phase and quadrature, edge-coupled orthogonal feed providing circular polarization (CP) in broadside ($\theta = 0°$, i.e., 90° elevation). In order to increase the sensitivity, a monolithic low-noise amplifier (LNA) was inserted at each patch output. The centers of the patches form a triangle, as shown in Fig. 1. One can notice that the triangle is not equilateral. This asymmetry results from design considerations on the mutual coupling between the elements and the orientation of the elements with respect to each other. In order to minimize the influence of the single-element pattern on the DF system performance, it was decided to use the same orientation for the three elements [as shown in Fig. 1(a)]. In this case, given the antenna dimensions and the topology of the feeding structure, an equilateral configuration would cause a strong coupling between the feed of antenna C and the two other patches. When a neural network is used to implement the array factor synthesis, there is a great flexibility in the position of the

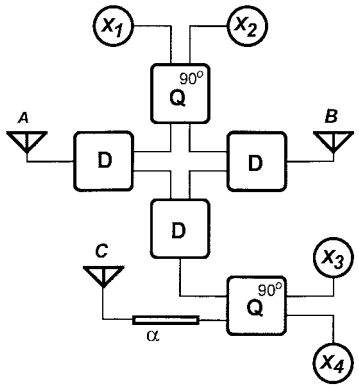

Fig. 2. RF combiner with delay line. Legend: D—Wilkinson divider; Q—Branch line coupler.

elements. For instance, it is possible to increase the physical distance between the array elements to minimize coupling in order to keep a good impedance matching and then train the NN to implement an array factor corresponding approximately to a closer antenna spacing. However, the distance between the patches, should be kept small in order to prevent grating lobes. Using patterns with only one major lobe makes it easier to identify the DOA without ambiguity over the full 360° azimuth sector. In other words, the structure of the neural network will be simpler and it will be easier to train.

The information on the DOA is present in the relative phases of signals A, B, and C received by associated elements. A combining circuit shown in Fig. 2 is used to generate beam functions X_1–X_4 that are given in (1)–(4)

$$X_1 = \frac{\|B + jA\|^2}{4} \tag{1}$$

$$X_2 = \frac{\|A + jB\|^2}{4} \tag{2}$$

$$X_3 = \frac{\left\|Ce^{j\alpha} + \left(\frac{A+B}{2}\right)\right\|^2}{2} \tag{3}$$

$$X_4 = \frac{\left\|Ce^{j\alpha} - \left(\frac{A+B}{2}\right)\right\|^2}{2}. \tag{4}$$

These four functions depend on the elevation (θ) and azimuth (φ) angles of the incident wave as well as the operating frequency. In the equations above, A, B, and C are the signals at the output of the LNA's connected to the corresponding antenna elements in Fig. 1(b). In Fig. 2, the Q boxes are 90° hybrid junctions and the D boxes are balanced Wilkinson power dividers. A delay line producing a frequency-dependent phase shift α is introduced in the path of signal C. For the purpose of the experimental validation in an anechoic chamber, Schottky diodes were used to monitor the output dc levels X_1–X_4. In practice, a heterodyne detection scheme could be implemented to reject out-of-band signals.

The calculated patterns of X_1–X_4 versus the azimuth angle ϕ for an elevation angle of 0° (i.e., $\theta = 90°$) are shown in Fig. 3. These patterns do not take into account the element pattern. The relative differences between the four signals are used to determine φ and the role of the NN will be to

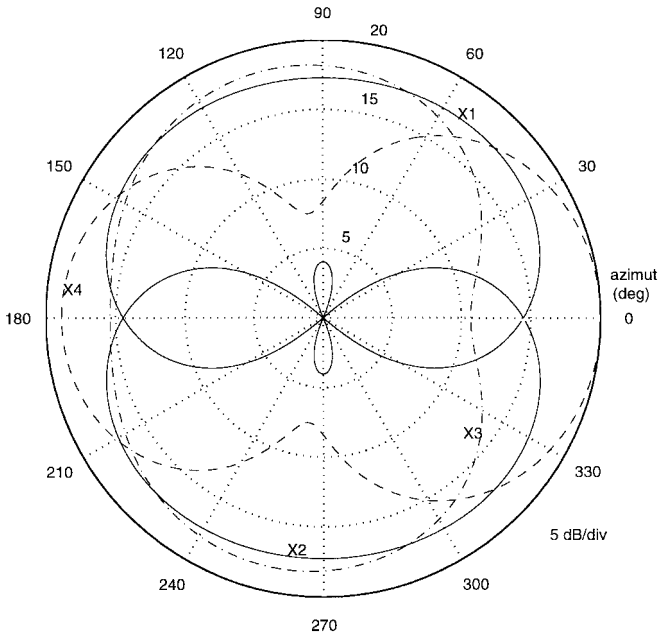

Fig. 3. Theoretical radiation pattern ($\theta = 90°$). Legend ——: X_1 and X_2; .-.-.-.: X_3; - - -: X_4.

synthesize a DOA function of the X_i variables, which has a smooth single-valued relationship with φ. For instance, the difference between X_4 and X_3 can indicate whether the source is on the left or the right side of the figure, but it is not possible to tell if it is located on the top or the bottom. Considering the difference between X_1 and X_2, it is possible to resolve this ambiguity. The training of the network will consist in the synthesis of the DOA function, which will be able to map the four X_i inputs onto φ with the greatest possible accuracy.

The nonlinear synaptic responses of the neurons contributes to the great training capabilities of NN-based classifiers. On the other hand, the direction predicted by the DOA circuit should not depend on the intensity of the incoming wave. This requires a way to normalize the X_i inputs with respect to the incident wave's power level. This level could be measured if one of the signals at the output of the combiner had an omnidirectional response over the full 360° sector. In general, it is very likely that none of the A, B, C, and X_i outputs will have an isotropic response. In this case, an optimally isotropic variable to be used as a normalization basis can be synthesized by using a single adaptive linear neuron (adaline) [10] performing a weighted sum of the four X_i values. Upon training, the adaline's output should be proportional to the incident wave's power and as much as possible not dependent on the DOA. In practice, the output of the adaline, defined as P_{in} could then feed directly to an automatic gain control stage to implement the normalization operation.

III. Beamforming Network

The architecture of the beamforming neural network (BFNN) shown on Fig. 4 consists of two MLP linked in parallel. Each MLP section comprises three neuron layers as can be seen in Fig. 5(a). The first layer consists of ten perceptrons with hyperbolic tangent activation functions. The

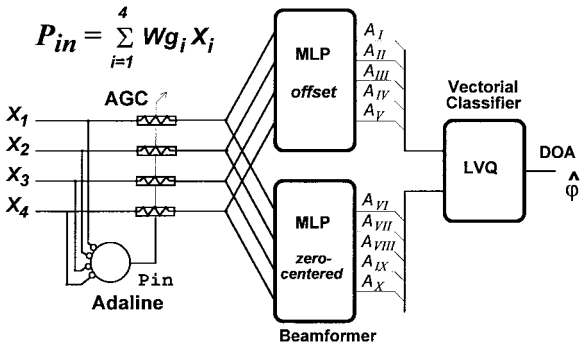

Fig. 4. Architecture of neural network DOA system.

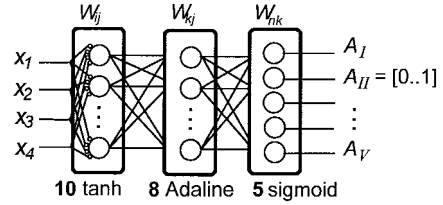

(a)

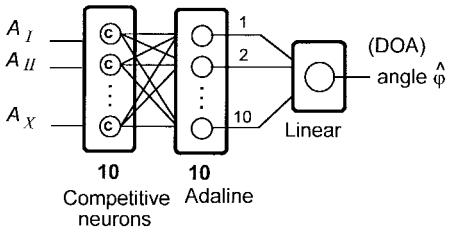

(b)

Fig. 5. (a) Schematic of the three-layer MLP. (b) Schematic of the LVQ network.

second layer consists of eight adalines and the output layer has five perceptrons with sigmoid activation functions whose outputs are between zero and one. The A_n outputs of the MLP are obtained from the X_i inputs according to the relationship

$$A_n = \mathbf{logsig}\left\{\sum_{k=1}^{8} W_{nk}\left(\sum_{j=1}^{10} W_{kj}\left[\sum_{i=1}^{4} \mathbf{tanh}(W_{ji}X_i + B_j)\right] + B_k\right) + B_n\right\}$$
$$n = \text{I, II, III, } \cdots\text{, IX, X} \tag{5}$$

where **logsig** is defined as

$$\mathbf{logsig}(x) = 1/\{1 + \exp(-x)\}$$

and W_{ji}, W_{kj}, and W_{nk} are the weights used in the first, second, and third layer, respectively, while B_j, B_k, and B_n are the corresponding activation thresholds. Each one of the ten A_n outputs is associated with a 72° azimuth sector. These sectors are defined in Fig. 6 and they form two sets of five overlapped sectors, each set covering 360°, and being shifted by 36° with respect to each other. As seen on the figure, any DOA will fall in two partially overlapping sectors. The network is trained in such a way that the outputs corresponding

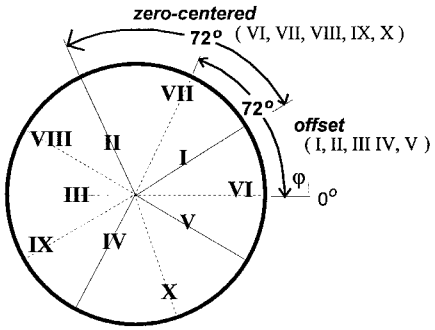

Fig. 6. Definition of the ten sectoral regions used by the azimuth classifier.

to these sectors will be activated (A_n close to one) while the others will not (A_n close to zero). The transitions from zero to one and one to zero on the A_n outputs are abrupt because in the learning phase, we train the MLP to follow as much as possible the desired output node responses defined as

$$\boldsymbol{n}\text{th desired output node response} = \begin{cases} 1 \text{ if DOA in } n\text{th } 72^\circ \text{ sector} \\ 0 \text{ if DOA not } n\text{th in } 72^\circ \text{ sector.} \end{cases}$$

By taking into account the 72° sectors' overlap, it should be possible to predict the DOA within an interval of 36° by appropriate processing of the A_n outputs. The advantage of splitting the beamforming circuit into two MLP sections taking decisions on 72° sectors, instead of having only one larger MLP taking decisions on 36° sectors, is noticeable at the training stage since both sections can be trained separately in parallel. With a unique larger MLP, the learning process would try to modify some insignificant synaptic weight connections. The network would take more time to learn, have more difficulty to converge to an optimal solution and could possibly get trapped in local minima. However, if we train two blocks separately, we constrain the network to have less degrees of freedom, and the number of unknown variables decreases considerably. Convergence may then be achieved more rapidly. The training process will be described in the next section. Since we wish to have abrupt zero-to-one transitions for the output node responses, MLP neurons were used instead of radial basis function to minimize the number of neurons.

A priori, if the A_n outputs really behaved as logic variables with sharp transitions between the zero and one states, it would be a simple task to identify a 36° interval belonging to two overlapping sectors containing the DOA with a circuit consisting of ten two-input AND gates. In practice, after training, each A_n still has a smooth continuous variation between 0 and 1 and a learning vector quantization (LVQ) was used. A ten-element vector A is formed with the A_n output levels. This vector is compared to each member in a set of reference vectors that represent the ideal 36° interval responses. If A is closely matched to one of the reference vectors, then the DOA is assumed to be in the corresponding 36° interval. For example, the reference vector associated with the 0°-to-36° interval in Fig. 6 is [1, 0, 0, 0, 0, 1, 0, 0, 0, 0] because this interval is common to sectors I and VI. The other reference vectors are similarly defined.

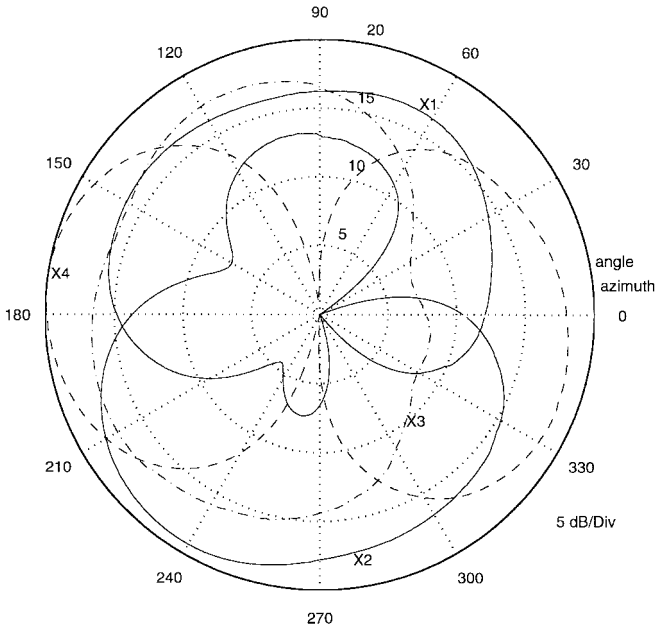

Fig. 7. Measured radiation patterns, output X_1–X_4 ($f = 1.55$ GHz and elevation $= 45^\circ$).

The network, shown in Fig. 5(b), computes the distance between the input vector Δ and reference vectors using competitive neurons. Upon training, the network will generate maximum likelihood decisions in a quasi-optimal fashion. The decision unit produces one out of ten discrete levels, these levels being respectively associated with each one of the 36° intervals. In the foregoing examples, the intervals are centered at 18°, 54°, 90°, $\cdots$, 342°.

Using the proposed hybrid architecture including an RF combining network followed by a NN, it is possible to classify the input signal into ten orthogonal sectors. An implementation of a classifier forming ten orthogonal beams using RF circuits only such as a Butler matrix would require a minimum of ten antenna elements. The NN approach used here needs a minimum of only three antenna elements. However, a Butler matrix could determine the direction of multipath beams arriving simultaneously. This is not possible with the proposed system due to the nonlinear processing of the received signals in the combining circuit (1)–(4) and in the MLP (5).

IV. Learning Strategy

In order to validate the concept, experiments were conducted in an anechoic chamber. The antenna described in Section II was illuminated by an incident CP beam and rotated with azimuth steps of 1° for fixed elevation angle (conical pattern). Altogether, five patterns were recorded with different frequencies and elevation angles. These patterns were used later for training. Fig. 7 gives the recorded patterns of outputs X_1–X_4 for an elevation angle of 45° and a plane wave frequency of 1.55 GHz. The patterns do not show four well-defined maximums separated by 90°, as in the ideal case simulated in Fig. 3. The distortions in the patterns are due to hardware imperfections such as the nonisotropic behavior of the radiating elements, parasitic coupling between the elements

and their feed lines, finite dimensions of the antenna ground plane, etc. It will be the task of the training process to compensate for these effects.

The azimuth angle of arrival φ depends on the X_i's via the characteristics of the RF combining circuit. However, for a given value of φ, each X_i depends on the frequency of the operation f and the elevation angle θ of the incident beam. Therefore, we can write

$$\varphi = g(X_1, X_2, X_3, X_4, f, \theta). \tag{6}$$

In practice, θ is not varying over a wide range for typical mobile communications with a geostationnary satellite or terrestrial base station. Also, the frequency of the pilot signals are generally stable and well defined. However, in order to assess the robustness of our DOA circuit to elevation and frequency variations, we have assumed that these variables could fluctuate. For that purpose, we have experimented with training under three different conditions:

1) $f = 1.55$ GHz, $\theta = 45°$, data set corresponding to 360 φ directions with 1° steps;
2) $f = 1.50, 1.55$, and 1.60 GHz, $\theta = 45°$, data set corresponding to 72 φ directions with 5° steps at each frequency (216 points);
3) $f = 1.55$ GHz, $\theta = 30, 45$, and $60°$, data set corresponding to 72 φ directions with 5° steps at each elevation θ (216 points).

The measured data sets consist of arrays of X_i vectors with $i = 1, 2, \cdots, 4$. Training the NN with the two last sets should lead to DOA circuits that are less sensitive to the fluctuations of the environment while the first condition should give a minimum number of erroneous decisions under good environmental conditions. The weights of the adaline at the NN input used to accomplish automatic level control were obtained after training with data sets 2 and 3 to provide more robustness. The training was performed with the Widrow–Hoff algorithm [7], [8]. Training of the MLP's was accomplished with the Levenberg–Marquart algorithm [11] according to the following equation:

$$\Delta W = \left[\frac{\partial \boldsymbol{e}}{\partial W}^T \bullet \frac{\partial \boldsymbol{e}}{\partial W} + \mu I \right]^{-1} \bullet \frac{\partial \boldsymbol{e}}{\partial W} \boldsymbol{e} \tag{7}$$

where μ is an adjustable parameter controlling the convergence rate. $\boldsymbol{e}$ is the residual vectorial error defined as $\boldsymbol{e} = \boldsymbol{T} - \boldsymbol{A}$, where $\boldsymbol{T}$ is the desired output vector and $\boldsymbol{A}$ is the vector of neurons' responses.

The Kohonen rule was subsequently used to train the LVQ decision unit described in the previous section that is

$$\Delta W_{ij} = l_r \cdot C_i \cdot [A_j - W_{ij}] \qquad \text{with } C_i = \begin{cases} +1, & \in \wp_i \\ -1, & \notin \wp_i \end{cases} \tag{8}$$

l_r is the learning rate (less than 1) and C_i is a constant that affects the winner neuron only [12]. The value of C_i (1 or -1) depends on the desired (or winning) neuron giving a true or false decision. A_j is the incoming input provided by the beamformer.

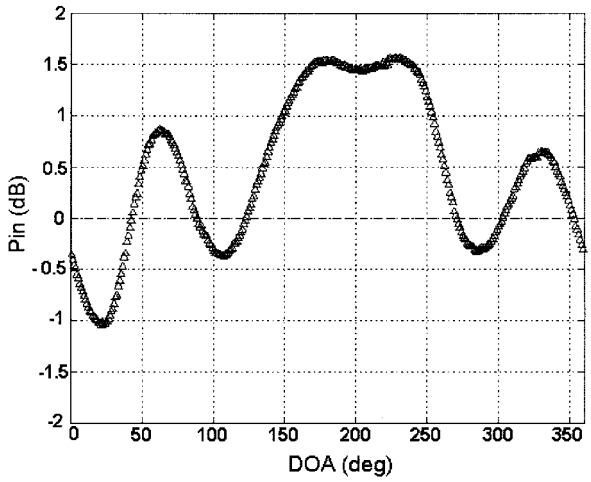

Fig. 8. Normalization constant P_{in} on a function of the DOA for a training at $f = 1.55$ GHz and elevation $= 45°$.

Upon training, we obtain a discrete estimated value of DOA computed from the outputs of the RF combiner

$$\hat{\varphi} = \mathbf{h}(X_1, X_2, X_3, X_4). \tag{9}$$

V. Experimental Results

In order to validate the direction finding algorithm, the X_i power vectors were measured under the various illumination conditions given in the previous section. These measurements were done in an anechoic chamber to minimize the occurrence of multipath. A spiral antenna was used to produce the incident CP wave. The power levels were in fact obtained from measured rectified dc voltage levels on diode detectors, by using a simple two-layer network to model the diode characteristics. Subsequently, a software implementation of the neural network, including the automatic gain control unit, was realized using the MATLAB® neural network toolbox. With adequate training, the network should be able to generalize and predict φ with the best possible accuracy. However, since the LVQ decision unit is designed to associate the DOA with a 36° interval, there is only a finite discrete set of predicted values. The training of the NN was accomplished by using the measured data directly.

The performance of the normalization adaline after training is shown in Fig. 8 where the normalization variable P_{in} is plotted versus φ. As we can see, there is still a residual fluctuation of ± 1 dB of P_{in}. This is expected given the variability of the X_i patterns shown in Fig. 7. Except for the tests in the presence of noise and interference, all validation scenarios to be presented in the following were repeated by artificially applying a 0, $+10$ and -10 dB gain to the X_i inputs in order to verify the capability of the NN function with nonideal normalization. There were no significant differences between the results obtained with the three gain values. Only the 0-dB gain results will be presented for brevity.

Three series of tests were first done without interference and noise in order to assess the capabilities of the system under such conditions. In each series, a new data set was used and a new training was performed. Only a subset of

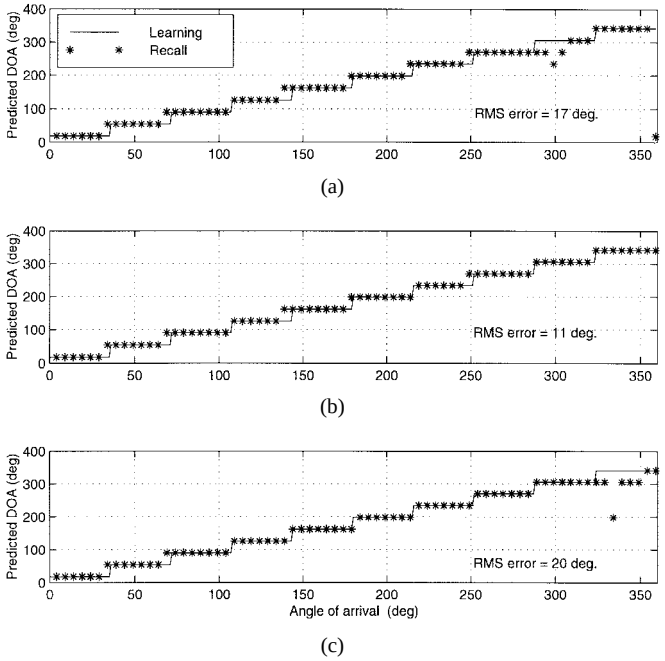

Fig. 9. Network recall for different frequencie. (a) Validation of learning at 1.50 GHz. (b) Validation at 1.55 GHz. (c) Validation at 1.60 GHz.

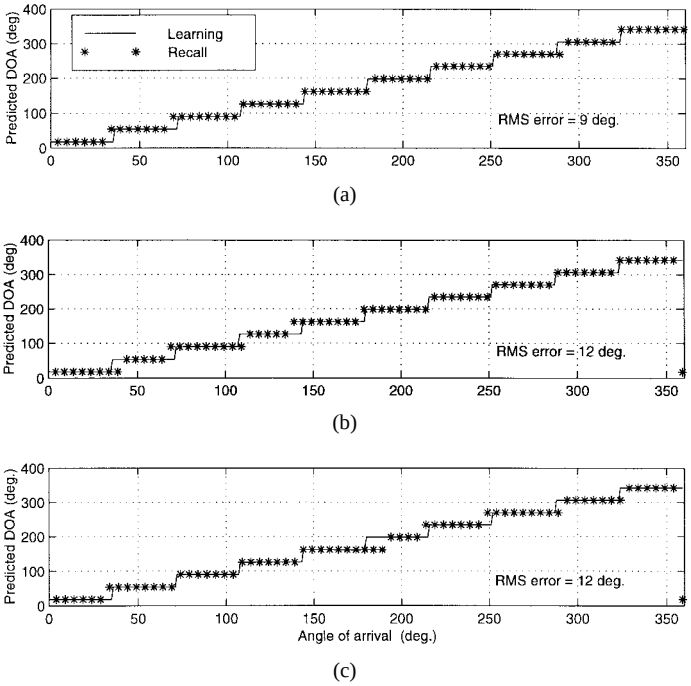

Fig. 10. Estimated direction of arrival (DOA) for different elevation angles: (a) 60°, (b) 45°, and (c) 30°.

the measured data was used for training and the entire set was used for testing. In the first series, only one elevation angle and one signal frequency were used for training and recall (data set #1). For this case, the predicted DOA sector was determined accurately for all DOA cases, indicating that the NN can compensate for the distortions in the radiation patterns measured at the output of the combiners.

In the second series of tests using data set #2, less training points were given and the signal frequency was allowed to vary. This variation introduces more distortions in the X_i patterns since all the RF components have a frequency dependent behavior. This is especially true for the patch antennas which are resonant structures. The predicted DOA obtained by recall of the trained network is shown as a function of the actual DOA in Fig. 9. It can be seen that the number of false predictions is quite small at the three training frequencies, which confirms the capability of the proposed circuit to work with broadband signals. However, in practical cases where a pilot signal is used for tracking, the frequency is accurately known and there is no need for such a broad-band robustness.

In the third series of tests (data set #3), the number of training points is again reduced compared to the first case and the frequency is fixed. In practice, the elevation of the incident beam used for tracking, with respect to the plane of the antenna, may vary with time. This should not affect the performance of the direction finding system. We have trained the neural network with three different elevation angles. Again, the predicted DOA's were in the appropriate sectors for most of the cases tested (see Fig. 10). It can be seen in Figs. 9 and 10 that the majority of the estimation errors occurs at the edges of the 36° intervals. This is a consequence of the limited sharpness of the node responses at the output of the MLP.

The direction finding method and the circuit we are proposing are static in the sense that the NN has its weights fixed until a new training sequence is initiated. This is in contrast with an adaptive approach in which the weights can be readjusted dynamically to account for the presence of interference [10], [13]. Furthermore, elaborate processing techniques can be implemented to separate the signal space from the noise (interference) space. Of course, in our circuit, signal and noise are integrated together by the diode detectors and such separation could be possible but with an amplitude modulated signal.

The effect of a second incident wave (interference signal), arriving with a direction ψ, was simulated by assuming that this interference was not coherent with the first incident beam arriving with a direction φ. Therefore, we can calculate the X_i values in presence of the two beams by simply adding the power levels obtained with each case taken separately. Adjusting the weight of the two contributions simply changes the signal-to-interference (S/I) ratio. For each S/I level, φ and ψ were both varied by 5° steps between 0° and 360° (72 × 72 points) and the DOA interval was estimated by the trained NN. A root mean square (rms) error on the DOA was calculated with the following formula:

$$\text{DOA error}_{(\text{RMS})} = \sqrt{\frac{1}{72}\sum_{\varphi}\cdot\frac{1}{72}\sum_{\psi}\left(\text{MOD}_{180^\circ}\left(|T_i - D_i|\cdot 36^\circ\right)\right)^2} \quad (10)$$

where D_i is the estimated 36° interval number and T_i is the actual interval number containing the desired signal arriving with an angle φ (consecutive intervals are numbered in a sequence from 1 to 10). The results for the three types of training are given in Fig. 11 showing the rms error as a function of S/I. It can be seen that the error stabilizes for

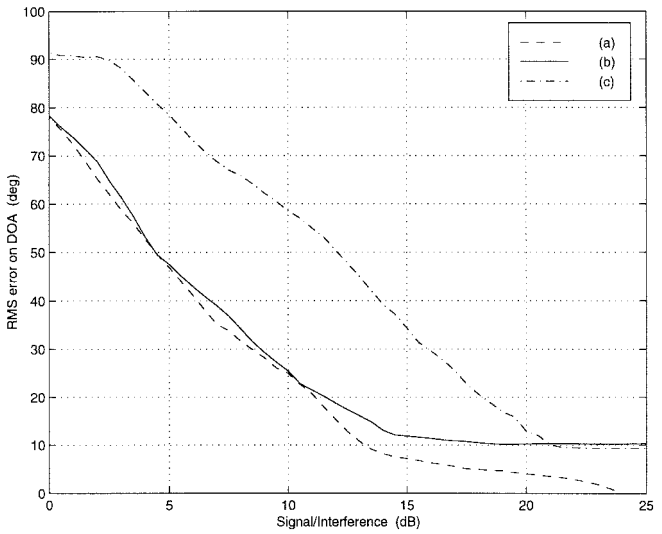

Fig. 11. Classifier performance in presence of interference. (a) $f = 1.55$ GHz and elevation $= 45°$. (b) $f = 1.50, 1.55$, and 1.60 GHz (elevation fixed to 45°). (c) Elevation $= 30°, 45°$, and $60°$ ($f = 1.55$ GHz).

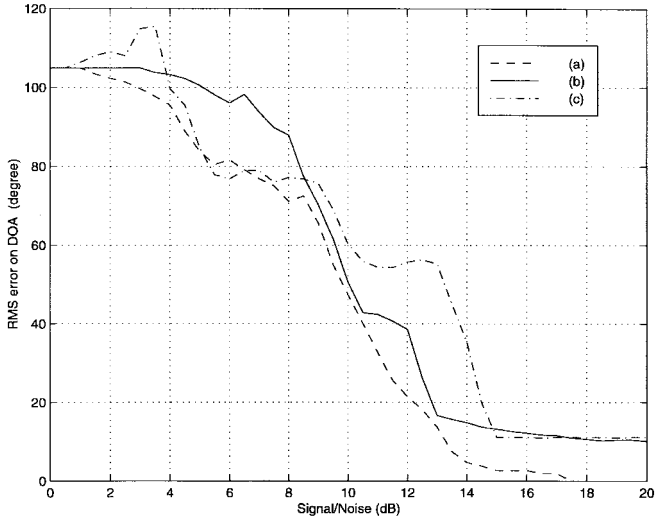

Fig. 12. Classifier performance in presence of noise. (a) $f = 1.55$ GHz and elevation $= 45°$. (b) $f = 1.50, 1.55$, and 1.60 GHz (elevation fixed to 45°), and (c) elevation $= 30°, 45°$, and $60°$ ($f = 1.55$ GHz).

S/I values greater than about 14.5 dB. As expected, the single angle-single frequency case (data set #1) is the most accurate.

The performance of the system was also verified in the case where a minimum detection floor is present. This can be the case when the signal strength is weak and the internal noise (e.g., thermal noise in the diodes) limits the dynamic range of the measurements. The same formula as above (10), but without the inner summation, was used to calculate the DOA error in presence of the noise floor. For each value N of noise floor, the power readings X_i that were smaller than N were assigned a value of N. The signal level S used to compute the signal-to-noise ratio (S/N) was taken as the largest X_i value measured at the four detectors, and for all the observation angles over the 360° range. Therefore, all the readings have an actual S/N ratio smaller than or equal to the ratios quoted on the horizontal axis in Fig. 12. As expected, when all the diodes have reached the signal noise floor (S/N $= 0$), the error is the same for all training strategies. As in the interference case, the error stabilizes near the no-noise value for an S/N level of about 14 dB. This is, therefore, the minimum dynamic range required to achieve optimum accuracy with our system. This should not be taken as an ultimate limitation and smaller dynamic ranges could probably be achieved with different RF circuit and neural network architectures.

VI. Conclusions

In this paper, we have presented an implementation of a DF system using a neural network to classify the direction of arrival into one of ten 36° intervals covering the full 360° azimuth range. The system presented uses a minimum of three antenna elements required to avoid a 180° ambiguity. The results have demonstrated the flexibility made available by the inherent training capabilities of the neural network. It was shown that by using sets of weights obtained by training under different conditions, it is possible to extend the direction finding capabilities to varying signal frequencies and elevation angles of the incident beam. Even more interesting is the fact that the training process can compensate for the unexpected performance of the RF hardware. This was important in our work where the small antenna platform used led to parasitic effects that caused significant degradation to the antenna patterns. Functions such as automatic gain control and linearization of diode characteristics were also conveniently implemented with basic neuron-based structures.

The proposed system uses a very simple RF circuit architecture including patch antennas, low-noise amplifiers, standard hybrid junctions, and diode detectors. In order to focus on the resolution capability of the neural network beamformer, no reference oscillator and frequency down-conversion were used to recover the in-band signal. Therefore, the noise and interference rejection capabilities are limited. The best performances were obtained for S/N and S/I of 14.5 dB or higher.

The use of a finite number of intervals in the beam classifier limits the accuracy on the DOA estimates to $\pm 18°$ in the case of the system presented. This is suitable for tracking applications using steerable medium-directivity antennas, as in land-mobile satellite communication terminals.

Acknowledgment

The authors would like to thank the anonymous reviewers for their positive comments and suggestions. They would also like to thank J. Gauthier for his help in the antenna fabrication and measurements.

References

[1] J. Huang and A. C. Densmore, "Microstrip Yagi array antenna for mobile satellite vehicle application," *IEEE Trans. Antennas Propagat.*, vol. 39, pp. 1024–1030, July 1991.

[2] R. C. Johnson and H. Jasik, *Antenna Engineering Handbook*, 3rd ed. New York: McGraw-Hill, 1993.

[3] R. Milne, "Performance and operational considerations in the design of vehicle antennas for mobile satellite communications," in *Proc. 4th Int. Mobile Satellite Conf.*, Ottawa, Canada, June 1995, pp. 329–333.

[4] C. D. McCarrick, "Mechanically-steered disk antenna for mobile satellite service," in *Proc. 4th Int. Mobile Satellite Conf.*, Ottawa, Canada, June 1995, pp. 345–350.
[5] S. Preston and D. V. Thiel, "Direction finding using a switched parasitic antenna array," in *IEEE AP-S Int. Symp.*, Montreal, Canada, July 1997, pp. 1024–1027.
[6] H. L. Southall, J. A. Simmers, and T. H. O'Donnell, "Direction finding in phased arrays with a neural network beamformer," *IEEE Trans. Antennas Propagat.*, vol. 43, pp. 1369–1374, Dec. 1995.
[7] A. H. Zooghby, C. G. Christodoulou, and M. Georgiopoulos, "Performance of radial basis function networks for direction of arrival estimation with antenna arrays," *IEEE Trans. Antennas Propagat.*, vol. 45, pp. 1611–1617, Nov. 1997.
[8] D. Torrieri and K. Bakhru, "Simplification of the MUSIC algorithm using a neural network," in *Proc. IEEE Military Communicat. Conf. MILCOM*, Piscataway, NJ, 1996, vol. 3, pp. 873–876.
[9] T. Lo, H. Leung, and J. Litva, "Radial basis function neural network for direction of arrivals estimation," *IEEE Signal Processing Lett.*, vol. 1, pp. 45–47, Feb. 1994.
[10] B. Widrow and S. D. Stern, *Adaptive Signal Processing.* Englewood Cliffs, NJ: Prentice-Hall, 1985.
[11] H. Demuth and M. Beale, *Neural Network Toolbox User's Guide.* Natick, MA: The Math Works Inc., 1995, version 2.0.
[12] S. Haykin, *Neural Networks, a Comprehensive Foundation.* New York: Macmillan, 1994, pp. 429–430.
[13] W.-H. Yang and P.-R. Chang, "Programmable switched-capacitor neural network for MVDR beamforming," *IEEE J. Ocean. Eng.*, vol. 21, pp. 77–84, Jan. 1996.

Éric Charpentier (M'99) received the B.Eng. and M.Sc.A. degrees in electrical engineering from Ecole Polytechnique de Montréal, Canada, in 1998.

He received the radio-amateur license in 1988. He is currently at SR Telecom Inc., Saint-Laurent, Quebec, Canada, as a Microwave Designer. His research interests include the design of low-profile antennas and the integration of subsystem circuits in radio transceiver with application in wireless communications for rural zones. His interests also include the application of active VHF–UHF antennas, signal processing, and phase-coherent radio receivers.

Jean-Jacques Laurin (M'86–SM'98) was born in Le Gardeur, Quebec, Canada, in 1959. He received the B.Eng. degree in engineering physics from Ecole Polytechnique de Montréal, Canada, in 1983, and the M.Sc.A. and Ph.D. degrees from the University of Toronto, Canada, both in electrical engineering, in 1986 and 1991, respectively.

He is now an Assistant Professor in the Department of Electrical and Computer Engineering, Ecole Polytechnique de Montreal, where he is a member of Poly-Grames Research Centre. During the academic year 1998–1999, he was an Invited Professor at Ecole Polytechnique Fédérale de Lausanne, Lausanne, Switzerland, where he worked in the Electromagnetics ans Acoustics Laboratory (LEMA). His research interests are in the areas of antenna design, modeling for antenna and electromagnetic compatibility applications, and near-field measurement techniques.

Dr. Laurin is a member of the Ordre des Ingénieurs du Québec.